Formation and Destabilization of the Particle Band on the Fluid-Fluid Interface

Jungchul Kim,[†] Feng Xu, and Sungyon Lee[*]
Department of Mechanical Engineering, Texas A&M University, College Station, Texas 77843, USA
(Received 5 August 2016; revised manuscript received 1 December 2016; published 13 February 2017)

An inclusion of particles in a Newtonian liquid can fundamentally change the interfacial dynamics and even cause interfacial instabilities. For instance, viscous fingering can arise even in the absence of the destabilizing viscosity ratio between invading and defending phases, when particles are added to the viscous invading fluid inside a Hele-Shaw cell. In the same flow configuration, the formation and breakup of a dense particle band are observed on the interface, only when the particle diameter d becomes comparable to the channel gap thickness h. We experimentally characterize the evolution of the fluid-fluid interface in this new physical regime and propose a simple model for the particle band that successfully captures the fingering onset as a function of the particle concentration and h/d.

DOI: 10.1103/PhysRevLett.118.074501

Controlling interfacial instabilities [1] is of critical importance in many engineering and geophysical processes, ranging from droplet microfluidics [2], lung airways [3,4], enhanced oil recovery [5], to volcanic flows [6]. The manipulation of viscous fingering was recently achieved by modulating the channel properties [7,8], or by employing time-dependent injection strategies [9].

The development in particle design and production provides another tool for modifying fluid-fluid interfaces [10–14]. For instance, when particles adsorb on the interface, they assemble into a dense monolayer via capillary attractions [15,16] and rigidify interfaces [16–21] against interfacial instabilities. The stabilizing effects of adsorbed particles on the interface have led to a number of technological advances, from stabilizing emulsions [22] to forming "liquid marbles" [23]. More recently, the wettability of particles was utilized to control viscous fingering, as Trojer and colleagues [24] suppressed viscous fingering by injecting air into a saturated packing of hydrophobic particles. In the reverse scenario, oil injection into a channel containing hydrophilic particles was shown to induce viscous fingering [25]. In all aforementioned studies, particles directly affect the surface energy of the interface.

Particles entrained in a fluid flow can also indirectly alter the interfacial dynamics and even cause or delay instabilities. Yet, only a limited number of studies examine this coupling between suspensions and fluid-fluid interfaces. For instance, the addition of particles to a viscous liquid is shown to accelerate the droplet pinch-off [26–31], and the exact physical mechanism remains unknown. Thin, free-surface flows of the negatively buoyant particle and oil mixture exhibit particle concentration-dependent fingering behaviors down an incline [32–41]. In particular, at high particle concentrations, fingering of the suspension-air interface becomes *suppressed* as particles aggregate near the free surface instead of settling. More recently, Kulkarni and colleagues [42] demonstrated that adding noncolloidal particles to a spreading thin film on a rotating surface can initially enhance fingering (resulting in shorter wavelengths), before unstable wavelengths increase at higher particle concentrations. This nonmonotonic dependence of fingering instability on the particle concentration alludes to the complex relationship between suspended particles and interfaces.

Distinct from previous examples of thin suspension flows that are inherently susceptible to fingering, particles immersed in a fluid can also *destabilize* the fluid-fluid interface that is otherwise stable, when the suspension is injected into a Hele-Shaw cell [43,45]. In this radial flow, particles accumulate near the interface, which locally increases the effective viscosity [43–45] and leads to miscible fingering inside the suspension [46]. The resultant inhomogeneous distribution of particles causes interfacial deformations, while the analogous experiments with a clear liquid exhibit stable, circular interfaces [Fig. 1(a)].

In this Letter, we focus on the destabilizing effect of particles on the fluid-fluid interface, as particles in a wetting liquid spontaneously form a dense band near the interface and break up into fingers in the radial source flow. This new fingering regime arises unexpectedly when the channel confinement becomes important, or if $d \sim h$, where d and h are the particle diameter and channel gap thickness, respectively. We experimentally observe the spreading of a mixture of oil and neutrally buoyant, noncolloidal particles in a Hele-Shaw cell, and quantify the onset of this particle band formation and breakup. Based on the rate of particle band growth as the suspension expands, a simple model successfully predicts this onset as a function of h/d and the suspension volume fraction ϕ_0.

As depicted in Fig. 1(b), the Hele-Shaw cell consists of two Plexiglas plates ($30.5 \times 30.5 \times 3.8$ cm) that are separated by h ranging from 0.2 to 1.4 mm. The silicone oil (density $\rho_l = 0.96$ g/cm^3 and viscosity $\mu_l = 0.096$ Pa · s, UCT) wets the cell walls and particles completely, so that particles remain immersed inside the liquid. Two sets of polyethylene particles

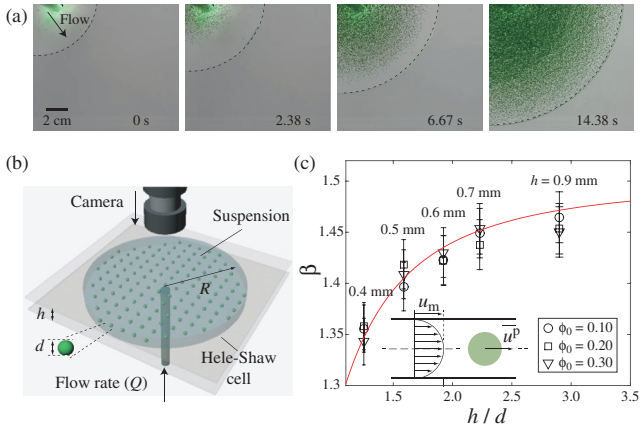

FIG. 1. (a) The sequence of images shows the particles "chasing" and "catching up" to the fluid-fluid interface when the pure oil is injected ahead of the particle-oil mixture; the dotted line indicates the location of the liquid-air interface. (b) Schematic of the experimental setup [45]: suspension is injected into the Hele-Shaw cell from the center, and experiments are recorded with the camera from above. (c) An analytical expression for the velocity ratio β as a function of h/d is plotted with experimental data for different values of ϕ_0 and h/d; the inset shows the schematic of a single particle moving with $\bar{u}^p$ at the channel centerline.

used (density $\rho_p = 1.00$ g/cm^3, Cospheric) have average diameters, $d = 330$ and 130 μm, respectively. The monodisperse suspension is injected into the center of the cell at a fixed flow rate Q with a syringe pump (New Era); ϕ_0 is varied from 0.05 to 0.35, while $Q = 30$–150 mL/ min (complete list of parameters in the Supplemental Material [47]). The particle-laden flow is recorded with a Canon 60D camera from above (1920 × 1080 pixel images, FOV 64°) at 30 frames/ sec, while an LED panel (EnvirOasis) illuminates the cell from below.

The key to interfacial instabilities is the accumulation of particles on the fluid-fluid interface that modifies the flow resistance near the interface [43–45]. Particles accumulate on the interface because they move faster than the mixture upstream of the interface, or $\beta \equiv \bar{u}^p/\bar{u} > 1$, where $\bar{u}^p$ and $\bar{u} = Q/(2\pi rh)$ correspond to the average particle and mixture velocities, respectively. This is clearly demonstrated in Fig. 1(a), in which particles "catch up" to the liquid-air interface when the pure oil is injected ahead of the suspension. For $h \gg d$, this net flux of particles is caused by "shear-induced migration" [48,49] that focuses particles towards the centerline due to particle-particle interactions in the Stokes regime.

Even as $h \sim d$, which eliminates particle-particle interactions, a single particle that moves near the centerline [inset of Fig. 1(c)] will move faster than $\bar{u}$ [50]. While the exact physical mechanism of particle focusing remains unclear in this "monolayer" limit, it may be attributed to non-negligible fluid inertia near the injection region [51–55]. Assuming that a particle reaches a quasi-steady velocity, $\bar{u}^p$, at the centerline, the force and torque balance on the particle in the Stokes regime [56–58] yields $\mu_l(u_m - \bar{u}^p)\pi d \sim \mu_l u_m d^3/h^2$, where $u_m = 3\bar{u}/2$ is the centerline speed of the undisturbed parabolic flow. Hence, $\beta = (3/2)[1 - \alpha(d/h)^2]$, where $\alpha = 0.16$ is an empirical constant. As shown in Fig. 1(c), the validity of β in the single particle limit is verified experimentally via particle tracking for varying ϕ_0 and h/d; in particular, β is independent of ϕ_0, distinct from its continuum counterpart that strongly varies with ϕ_0 [45].

In the ϕ_0-h/d parameter range with no particle accumulation, the interface remains circular, referred to as a stable "no fingering" regime [see Fig. 2(a)]. As ϕ_0 increases at given h/d, gradual particle accumulation is observed and yields an increase in the flow resistance, or reduced mobility, M, near the interface. This local decrease in M leads to miscible viscous fingering and formation of particle clusters inside the suspension, analogous to classical viscous fingering that is caused by a less viscous fluid (higher M) displacing a more viscous one (lower M) [46,59,60]. The appearance of the particle clusters coincides with slight interfacial deformations, as previously observed in [43–45] [denoted as "weak fingering" in Fig. 2(a)].

As ϕ_0 increases even above 0.4, the particle enrichment on the interface will inevitably approach the maximum packing fraction, $\phi_m \sim 0.6$. However, uniquely when $d \sim h$, this densely packed limit is reached even with

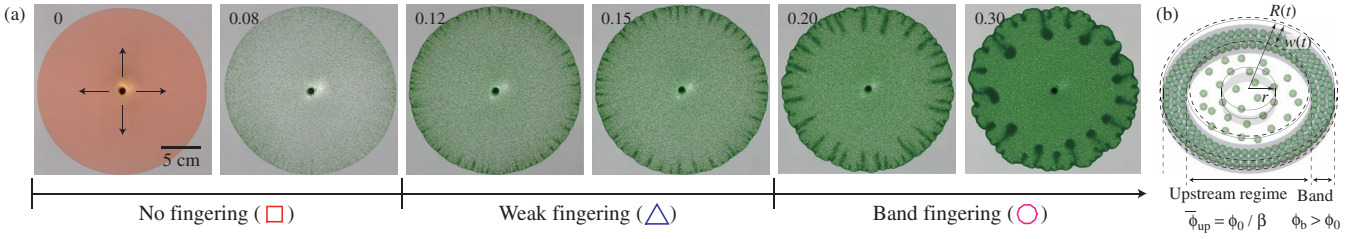

FIG. 2. (a) Fingering phenomena depend on the initial particle volume fraction, ϕ_0, at given $h/d = 3.5$: At small ϕ_0, the distribution of suspension remains uniform (no fingering regime); interfacial deformations are first observed at $\phi_0 = 0.12$ (weak fingering) and become more pronounced as ϕ_0 increases in the band fingering regime. The black arrows in the pure oil case indicate the flow direction. (b) Schematic of the particle band of width $w(t)$ and the concentration $\phi_b \approx 0.5$, and the upstream regime in which the particle concentration is given by $\bar{\phi}_{up} = \phi_0/\beta$.

relatively dilute input particle concentrations (i.e., $\phi_0 \approx 0.2$ for $h/d \approx 2$) and is marked by a sudden jump in ϕ, in lieu of the gradual particle accumulation that is unequivocally observed in the continuum limit. This discrete torus band of particles with a fixed volume fraction $\phi_b \lesssim \phi_m$ subsequently breaks to form particle-laden fingers in a so-called "band fingering" regime. As depicted in Fig. 3(b), this band breaking is preceded by miscible fingering between the displacing suspension and particle band, due to the jump in M. Afterwards, the interface tends to recover its circular shape due to the stabilizing viscosity ratio between the suspension and air, but slight interfacial deformations persist (in a manner similar to weak fingering) as particles continue to accumulate on the interface and cause miscible fingering.

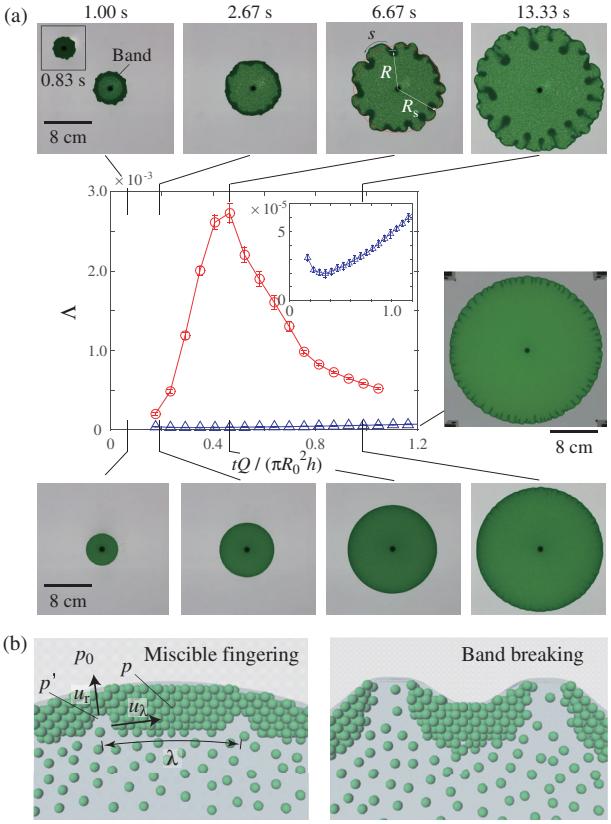

FIG. 3. (a) The plot of the interfacial deviation from a circle Λ over dimensionless time $tQ/(\pi R_0^2 h)$, where $R_0 = 10$ cm. Two rows of time-sequential images correspond to $h/d = 3.5$ (top) and 8.2 (bottom), respectively, while all other experimental values remain the same (i.e., $\phi_0 = 0.3$). The peak in Λ (circle) is only observed for the large particle case and coincides with the moment at which the particle band breaks. For $h/d = 8.2$, particles gradually accumulate on the interface, which leads to weak fingering; the value of Λ (triangle) is much lower than the large particle counterpart. (b) Schematic illustrating the sequence of events that lead to fingering: the jump in particle concentration between the displacing suspension and particle band leads to miscible fingering, resulting in the band break-up and pronounced fingers.

This evolution in the interfacial shape is quantified by the dimensionless interfacial deviation from a circle, $\Lambda = S^{-1}\int_S [1-(R/R_s)]^2 ds$ [44,45]. Here, R_s is the radius of the best fitted circle; s refers to the curvilinear coordinate defined along the interface, while R is the center-to-edge distance. A clear peak in Λ in Fig. 3(a) for $\phi_0 = 0.3$ and $h/d = 3.5$ (circle) corresponds to the moment at which the particle band breaks and is unique to the band breaking regime. When h/d increases to 8.2 while other parameters remain unchanged, particles gradually accumulate on the interface and yield weak fingering; the corresponding magnitude of Λ (triangle) is much lower than the band fingering counterpart. In addition to Λ, the contrast between weak fingering (bottom row) and band fingering (top row) is visually demonstrated in two sets of time-sequential images for $\phi_0 = 0.3$ in Fig. 3(a). The dense particle band clearly appears upon injection at $h/d = 3.5$ (top row), while only gradual concentration increase is observed at $h/d = 8.2$ (bottom row).

Why does the formation of the discrete particle band strongly depend on h/d? For $d \ll h$, a secondary flow near the interface, known as "fountain flow" [61], "sweeps" the incoming particles away from the interface, leading to the gradual particle accumulation when $\beta > 1$. However, for larger d/h, fountain flow can no longer effectively diffuse particles and yields the shocklike formation of the particle-rich region near the interface. Based on the characteristic length scale of the fountain flow [61], the minimum particle diameter must satisfy $d/h \gtrsim 0.2$ to suppress the fountain flow and enable band formation (see Supplemental Material [47] for details). The initial formation of the particle band is also aided by the particle accumulation on the free surface inside a tube, as previously observed in Refs. [61–63]. When the particle-rich free surface inside the tube expands into the Hele-Shaw cell, large values of d/h and ϕ_0 correspond to the scenario in which a large amount of particles is pumped into a highly confining channel and is more likely to form a dense band of particles.

Prior to destabilization, the time evolution of the particle band is computed by balancing the time-rated change in band volume $V_b(t)$, with the net flux of particles into the band at $R - w$ [schematic in Fig. 2(b)]:

$$\phi_b \frac{dV_b}{dt} = 2\pi(R-w)h\bar{\phi}_{\mathrm{up}}(\bar{u}^p - \bar{u})|_{R-w}, \qquad (1)$$

where the depth-averaged volume fraction $\bar{\phi}_{\mathrm{up}}$ upstream of the band is given by ϕ_0/β, based on mass conservation in the upstream regime [45] [Fig. 2(b)]. The solution to Eq. (1) yields

$$\Delta V_b = V_b(t) - V_b(t_i) = \frac{\phi_0}{\phi_b}\left(1 - \frac{1}{\beta}\right) Q(t - t_i), \qquad (2)$$

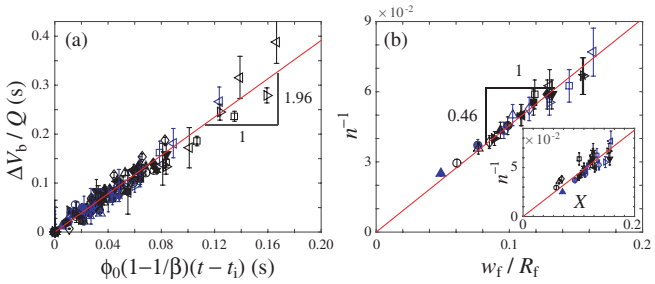

FIG. 4. (a) The experimental data of the change in the particle band volume ΔV_b are shown to follow Eq. (2). (b) The inverse of the wave number n^{-1} linearly scales with the ratio of the critical band width to the critical radius w_f/R_f. The inset consists of the plot of n versus $X \equiv 1-\sqrt{[1-(R_i/R_f)^2](1-\zeta)}$, where $\zeta \equiv (\phi_0/\phi_b)(1-\beta^{-1})$ (symbols listed in the Supplemental Material [47]).

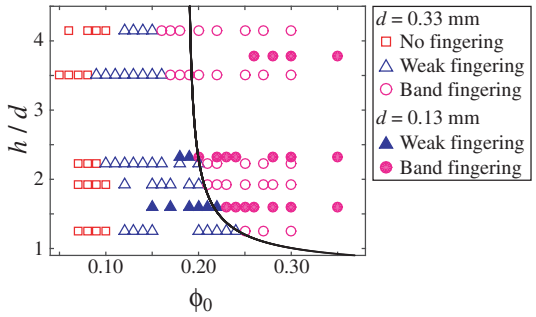

FIG. 5. All experimental runs are organized into a phase diagram that shows the dependence of fingering instability on ϕ_0 and h/d: no fingering (square), weak fingering (triangle), and band fingering (circle). The function of $\Pi = 0.63$ correctly captures the transition between weak and band fingering, especially in the limit of $h/d \sim 1$.

where t_i is the initial time of band formation. Figure 4(a) shows the experimental data of ΔV_b in good agreement with Eq. (2), which indicates that $\phi_b \approx 0.5$ slightly lower than ϕ_m.

The particle band of width $w(t_f) = w_f$ destabilizes and breaks at $R(t_f) = R_f$, where t_f corresponds to the time when miscible fingering initiates. A perturbation inside the band gives a rise in pressure p', which generates anomalous radial and tangential flows [see schematic in Fig. 3(b)] [64]. Based on Darcy's law, the radial growth speed relative to the band speed is given by $u_r \sim M_b[(p'-p_0)-(p-p_0)]/w_f = M_b(p'-p)/w_f$, where M_b is the mobility coefficient of band region, and p corresponds to the pressure inside the unperturbed band. The tangential growth speed is given by $u_\lambda \sim 2M_b(p'-p)/\lambda$, where λ is the wavelength. If we assume that the aspect ratio w_f/λ scales as u_r/u_λ, $\lambda \sim w_f$, independent of R_f, or $n^{-1} \sim w_f/R_f$, where the wave number $n = 2\pi R_f/\lambda$. Interestingly, this R_f or length-independent behavior of λ is analogously observed in wrinkling of thin, elastic membranes afloat on a gel or a liquid, in which $\lambda \propto \text{thickness}^{1/4}$, independent of the membrane length [65,66].

Combining Eq. (2) with $V_b = \pi[R^2-(R-w)^2]h$ yields

$$\left(1-\frac{w_f}{R_f}\right)^2 \approx \left(1-\left(\frac{R_i}{R_f}\right)^2\right)\left[1-\frac{\phi_0}{\phi_b}\left(1-\frac{1}{\beta}\right)\right], \quad (3)$$

where $Q(t_f-t_i) = \pi h(R_f^2-R_i^2)$, and $R(t_i) = R_i$ (detailed derivation in Supplemental Material [47]). Rearranging Eq. (3) yields the dependence of n on the relative band thickness w_f/R_f or $X \equiv 1-\sqrt{[1-(R_i/R_f)^2](1-\zeta)}$, where $\zeta \equiv (\phi_0/\phi_b)(1-\beta^{-1})$, which is experimentally validated in Fig. 4(b). Interestingly, in the limit of $(R_i/R_f)^2 \ll 1$, $n^{-1} \sim 1-\sqrt{1-\zeta}$, so that n can be determined based on the input parameters ϕ_0 and h/d.

In order to identify the band breaking criterion, we focus on the sustainability of the particle band, under the constraint that $w \gtrsim d$. In order to sustain the band of $w \sim d$, the particle flux at R_i must exceed the rate at which the particle band expands with the local flow $Q/(2\pi R_i h)$ or $\phi_b Q d/R_i \leq Q\phi_0(1-\beta^{-1})$. This inequality can be summarized in $\Pi \equiv n_m(\phi_0/\phi_b)(1-\beta^{-1})$, where $n_m \sim R_i/d$ is the wave number upon breaking of the thinnest band: For $\Pi \gtrsim 1$, band fingering is more likely to occur as the requirement for sustaining an initial particle band has been met, while, for $\Pi \lesssim 1$, band fingering cannot occur. As shown in the phase diagram of Fig. 5, the curve of $\Pi = 0.63$ successfully captures the boundary between the band fingering and weak fingering when $n_m \sim 5$ and shows that this simple model exhibits the correct functional dependence of the band fingering onset on ϕ_0 and h/d.

In-depth understanding of the band breaking regime enables the potential control of particle-induced viscous fingering. For instance, as $\lambda \sim w_f(\phi_0, h/d)$, which was also observed in the gravity-driven suspension [37], band fingering may be suppressed by strategically choosing ϕ_0 and the particle diameter, such that λ is larger than the channel width. Another striking feature of the band fingering regime is the particle pattern formation inside the suspension. Particle clusters that form upon the band breakup elongate and erode as the interface expands. They further divide into secondary clusters, which directly correlates to tip splitting and generation of secondary interfacial fingers. On-going studies include the modeling of this dynamic coupling between particle pattern formations and interfacial deformations, as well as the self-segregation and fingering of bidisperse suspensions. The present research is applicable to a diverse set of engineering processes that involve thin, particle-laden flows, such as spreading of suspension drops [67,68] and evaporation of complex liquids, such as blood [69], that exhibit coffee-ring effects [70].

The authors wish to thank Dr. Harry Swinney (UT Austin), Dr. Michael Allshouse (Northeastern), and

Dr. Tony Yu for their generous help in setting up the experimental apparatus. The financial support for this work was provided by the Texas A&M Engineering Experiment Station.

*sungyon.lee@tamu.edu
†Present address: Department of Extreme Thermal Systems, Korean Institute of Machinery & Materials, Daejeon 34103, Korea.

[1] L. Johns and R. Narayanan, *Interfacial Instability* (Springer, New York, 2002).
[2] C. N. Baroud, F. Gallaire, and R. Dangla, Lab Chip **10**, 2032 (2010).
[3] D. Huh, H. Fujioka, Y.-C. Tung, N. Futai, R. Paine, J. B. Grotberg, and S. Takayama, Proc. Natl. Acad. Sci. U.S.A. **104**, 18886 (2007).
[4] J. Grotberg and O. Jensen, Annu. Rev. Fluid Mech. **36**, 121 (2004).
[5] L. Lake, *Enhanced Oil Recovery* (Prentice Hall, Englewood Cliffs, NJ, 1989).
[6] K. Cashman and R. Sparks, Geol. Soc. Am. Bull. **125**, 664 (2013).
[7] T. T. Al-Housseiny, P. A. Tsai, and H. A. Stone, Nat. Phys. **8**, 747 (2012).
[8] D. Pihler-Puzović, P. Illien, M. Heil, and A. Juel, Phys. Rev. Lett. **108**, 074502 (2012).
[9] Z. Zheng, H. Kim, and H. A. Stone, Phys. Rev. Lett. **115**, 174501 (2015).
[10] L. Hong, S. Jiang, and S. Granick, Langmuir **22**, 9495 (2006).
[11] S. C. Glotzer and M. J. Solomon, Nat. Mater. **6**, 557 (2007).
[12] S. Jiang, Q. Chen, M. Tripathy, E. Luijten, K. S. Schweizer, and S. Granick, Adv. Mater. **22**, 1060 (2010).
[13] J. W. J. de Folter, M. W. M. van Ruijven, and K. P. Velikov, Soft Matter **8**, 6807 (2012).
[14] P. J. Lu and D. A. Weitz, Annu. Rev. Condens. Matter Phys. **4**, 217 (2013).
[15] P. Singh and D. D. Joseph, J. Fluid Mech. **530**, 31 (2005).
[16] D. Vella, P. D. Metcalfe, and R. J. Whittaker, J. Fluid Mech. **549**, 215 (2006).
[17] P. Pieranski, Phys. Rev. Lett. **45**, 569 (1980).
[18] E. H. Mansfield, H. R. Sepangi, and E. A. Eastwood, Phil. Trans. R. Soc. A **355**, 869 (1997).
[19] P. A. Kralchevsky and K. Nagayama, Adv. Colloid Interface Sci. **85**, 145 (2000).
[20] C. Planchette, E. Lorenceau, and A. L. Biance, Soft Matter **8**, 2444 (2012).
[21] M. Abkarian, S. Protière, J. M. Aristoff, and H. A. Stone, Nat. Commun. **4**, 1895 (2013).
[22] S. U. Pickering, J. Chem. Soc. Dalton Trans. **91**, 2001 (1907).
[23] P. Aussillous and D. Quéré, Nature (London) **411**, 924 (2001).
[24] M. Trojer, M. L. Szulczewski, and R. Juanes, Phys. Rev. Applied **3**, 054008 (2015).
[25] I. Bihi, M. Baudoin, J. E. Butler, C. Faille, and F. Zoueshtiagh, Phys. Rev. Lett. **117**, 034501 (2016).
[26] R. J. Furbank and J. F. Morris, Phys. Fluids **16**, 1777 (2004).
[27] R. J. Furbank and J. F. Morris, Int. J. Multiphase Flow **33**, 448 (2007).
[28] C. Bonnoit, T. Bertrand, E. Clément, and A. Lindner, Phys. Fluids **24** (2012).
[29] T. Bertrand, C. Bonnoit, E. Clément, and A. Lindner, Granular Matter **14**, 169 (2012).
[30] M. Z. Miskin and H. M. Jaeger, Proc. Natl. Acad. Sci. U.S.A. **109**, 4389 (2012).
[31] M. van Deen, T. Bertrand, N. Vu, D. Quéré, E. Clément, and A. Lindner, Rheol. Acta **52**, 403 (2013).
[32] J. Zhou, B. Dupuy, A. L. Bertozzi, and A. E. Hosoi, Phys. Rev. Lett. **94**, 117803 (2005).
[33] T. Ward, C. Wey, R. Glidden, A. E. Hosoi, and A. L. Bertozzi, Phys. Fluids **21**, 083305 (2009).
[34] B. P. Cook, Phys. Rev. E **78**, 045303 (2008).
[35] N. Murisic, J. Ho, V. Hu, P. Latterman, T. Koch, K. Lin, M. Mata, and A. L. Bertozzi, Physica (Amsterdam) **240D**, 1661 (2011).
[36] N. Murisic, B. Pausader, D. Peschka, and A. L. Bertozzi, J. Fluid Mech. **717**, 203 (2013).
[37] A. Mavromoustaki and A. L. Bertozzi, J. Eng. Math. **88**, 29 (2014).
[38] L. Wang and A. L. Bertozzi, SIAM J. Math. Anal. **74**, 322 (2014).
[39] S. Lee, Y. Stokes, and A. L. Bertozzi, Phys. Fluids **26**, 043302 (2014).
[40] S. Lee, A. Mavromoustaki, G. Urdaneta, K. Huang, and A. L. Bertozzi, Granular Matter **16**, 269 (2014).
[41] S. Lee, J. Wong, and A. Bertozzi, in *Mathematical Modelling and Numerical Simulation of Oil Pollution Problems*, edited by M. Ehrhardt (Springer, New York, 2015).
[42] M. Kulkarni, S. Sahoo, P. Doshi, and A. V. Orpe, Phys. Fluids **28**, 063303 (2016).
[43] H. Tang, W. Grivas, D. Homentcovschi, J. Geer, and T. Singler, Phys. Rev. Lett. **85**, 2112 (2000).
[44] A. Ramachandran and D. T. Leighton, J. Rheol. **54**, 563 (2010).
[45] F. Xu, J. Kim, and S. Lee, J. Non-Newtonian Fluid Mech. **238**, 92 (2016).
[46] G. M. Homsy, Annu. Rev. Fluid Mech. **19**, 271 (1987).
[47] See Supplemental Material at http://link.aps.org/supplemental/10.1103/PhysRevLett.118.074501 for a list of experimental parameters, additional derivations, and experimental images and videos.
[48] D. Leighton and A. Acrivos, J. Fluid Mech. **181**, 415 (1987).
[49] R. J. Phillips, R. C. Armstrong, R. A. Brown, A. L. Graham, and J. R. Abbott, Phys. Fluids **4**, 30 (1992).
[50] M. L. Ekiel-Jeżewska, E. Wajnryb, J. Bławzdziewicz, and F. Feuillebois, J. Chem. Phys. **129**, 181102 (2008).
[51] G. Segré, Nature (London) **189**, 209 (1961).
[52] G. Segré and A. Silberberg, J. Fluid Mech. **14**, 115 (1962).
[53] G. Segré and A. Silberberg, J. Fluid Mech. **14**, 136 (1962).
[54] D. Di Carlo, D. Irimia, R. G. Tompkins, and M. Toner, Proc. Natl. Acad. Sci. U.S.A. **104**, 18892 (2007).
[55] D. Di Carlo, J. F. Edd, K. J. Humphry, H. A. Stone, and M. Toner, Phys. Rev. Lett. **102**, 094503 (2009).
[56] V. R. Simha, Kolloid Z. **76**, 16 (1936).

[57] F. Gauthier, H. L. Goldsmith, and S. G. Mason, Trans. Soc. Rheol. **15**, 297 (1971).
[58] J. Happel and H. Brenner, *Low Reynolds Number Hydrodynamics* (Martinus Nijhoff Publishers, The Hague, 1981).
[59] P. G. Saffman and G. I. Taylor, Proc. R. Soc. A **245**, 312 (1958).
[60] L. Paterson, J. Fluid Mech. **113**, 513 (1981).
[61] A. Karnis and S. G. Mason, J. Colloid Interface Sci. **23**, 120 (1967).
[62] B. K. Chapman, Ph.D. thesis, University of Notre Dame, Notre Dame, IN, 1990.
[63] A. Ramachandran and D. T. Leighton, J. Rheol. **51**, 1073 (2007).
[64] S. S. S. Cardoso and A. W. Woods, J. Fluid Mech. **289**, 351 (1995).
[65] L. Pocivavsek, R. Dellsy, A. Kern, S. Johnson, B. Lin, K. Y. C. Lee, and E. Cerda, Science **320**, 912 (2008).
[66] H. Diamant and T. A. Witten, Phys. Rev. Lett. **107**, 164302 (2011).
[67] M. Nicolas, J. Fluid Mech. **545**, 271 (2005).
[68] V. Grishaev, C. S. Iorio, F. Dubois, and A. Amirfazli, Langmuir **31**, 9833 (2015).
[69] D. Brutin, B. Sobac, and C. Nicloux, J. Heat Transfer **134**, 061101 (2012).
[70] R. D. Deegan, O. Bakajin, T. F. Dupont, G. Huber, S. R. Nagel, and T. A. Witten, Nature (London) **389**, 827 (1997).